The importance of anisotropy in modeling ST segment shift in subendocardial ischaemia

The Importance of Anisotropy in Modeling ST Segment Shift in Subendocardial Ischaemia

Peter R. Johnston*, David Kilpatrick, and Chuan Yong Li

***Abstract*—In this paper, a simple mathematical model of a slab of cardiac tissue is presented in an attempt to better understand the relationship between subendocardial ischaemia and the resulting epicardial potential distributions. The cardiac tissue is represented by the bidomain model where tissue anisotropy and fiber rotation have been incorporated with a view to predicting the epicardial surface potential distribution. The source of electric potential in this steady-state problem is the difference between plateau potentials in normal and ischaemic tissue, where it is assumed that ischaemic tissue has a lower plateau potential. Simulations with tissue anisotropy and no fiber rotation are also considered.**

Simulations are performed for various thicknesses of the transition region between normal and ischaemic tissue and for various sizes of the ischaemic region. The simulated epicardial potential distributions, based on an anisotropic model of the cardiac tissue, show that there are large potential gradients above the border of the ischaemic region and that there are dips in the potential distribution above the region of ischaemia. It could be concluded from the simulations that it would be possible to predict the region of subendocardial ischaemia from the epicardial potential distribution, a conclusion contrary to observed experimental data. Possible reasons for this discrepancy are discussed.

In the interests of mathematical simplicity, isotropic models of the cardiac tissue are also considered, but results from these simulations predict epicardial potential distributions vastly different from experimental observations. A major conclusion from this work is that tissue anisotropy and fiber rotation must be included to obtain meaningful and realistic epicardial potential distributions.

***Index Terms*—Anisotropy, bidomain model, simulation, ST depression, subendocardial ischaemia.**

I. Introduction

ELECTROCARDIOGRAPHIC (ECG) ST segment depression has long been recognized as a sign of ischaemia [1], but the explanations of the responsible mechanisms have been controversial [2]. In this paper, we present a simple mathematical model of a slab of cardiac tissue in an attempt to further our understanding of the relationship between subendocardial ischaemia and the resulting epicardial potential distributions.

The model is based on the bidomain representation of cardiac tissue [3] which allows differing electrical conductivity in the intracellular and extracellular spaces as well as in the longitudinal and transverse directions. The model also incorporates cardiac fiber rotation between the endocardium and the epicardium.

The bidomain model has been used extensively in the study of electrical propagation along single fibers [4], [5], through bundles of cardiac fibers [4], [6], [7], through thin layers of cardiac cells [8] and even through the whole heart [9]. It has also been used to study the electrical fields created in the heart muscle as a result of ventricular defibrillation [10]. However, very few modeling studies have used the bidomain model in the study of ST segment shift. Such a study is steady-state in nature as the potential distribution arises from differing plateau potentials between normal and ischaemic tissue. On the other hand, propagation studies are, by necessity, transient. The ST segment studies of Holland and Brooks [11] and Smith *et al.* [12] use a spherical model of the heart yet ignore tissue anisotropy and fiber rotation. This paper also considers the effect making these simplifications has on the resulting epicardial potential distribution.

ST segment shift shown as ST depression in the ECG arises due to the currents set up in cardiac tissue flowing between normal and ischaemic muscle. The currents are induced by the difference between the plateau of the action potentials in normal and ischaemic tissues. This source essentially generates ST elevation over ischaemic tissue compared with normal tissue. How this is observed on the body surface depends on its position within the heart. There is a clear relationship between full-thickness ischaemia and epicardial ST elevation, which can also be observed on the body surface. When the ischaemic tissue is subendocardial i.e., does not reach the epicardium, there is ST depression observed both on the epicardium and on the body surface [13]. There is ST elevation on the endocardium over the ischaemic tissue, and this can sometimes be seen on the 12 lead electrocardiogram in leads such as aVR. The mechanism by which the endocardial ST elevation is expressed as ST depression on the epicardium is still unclear, and it is this difficulty which we expand in this paper.

A combined simulation/experimental study has been published by this group [13]. This study measured the potentials showing similar regions of ST depression on the epicardium for ischaemia in both the left anterior descending territory and the circumflex territory. The source was endocardial ST elevation in the ischaemic region as would be predicted. Observed epicardial ST changes, however, remained in the same position even when the epicardium was isolated, ruling out the explanation that the current flowed out the great vessels back on to the epicardium. Detailed modeling reproduced the same results but did not enable a simple explanation as to why the ischaemic region on the epicardium was centered over the boundary between the ischaemic and nonischaemic

Manuscript received August 10, 2001. This work was supported by the National Health and Medical Research Council of Australia and the National Heart Foundation of Australia. *Astertisk indicates corresponding author*

*P. Johnston is with the School of Science, Griffith University, Nathan, Queensland 4111, Australia (e-mail: P.Johnston@mailbox.gu.edu.au).

D. Kilpatrick is with the Discipline of Medicine, University of Tasmania, GPO Hobart, Tasmania 7001, Australia.

C. Li is with the Department of Physics, Nankai University, Tianjin, 300071, P. R. China.

Publisher Item Identifier S 0018-9294(01)10245-4.

regions. The modeling data suggested a powerful current sink at the boundary but gave no clue as to why this should be so. The work presented here originated from our need to further understand the nature of the subendocardial source. The underlying assumptions of the modeling in the above paper were that, although it contained a realistic cardiac geometry, fiber rotation was ignored. Also, by virtue of the fact that the simulations were purely numerical, the current source due to the ischaemic boundary was calculated from discrete values of the transmembrane potential. Here, although the geometry is simple, fiber rotation will be included and the current source will be treated in a continuous fashion.

II. Methods

A. Governing Equations

For the simulations performed here, it is assumed that the cardiac tissue can be represented by a block of tissue, infinite in the x and y coordinate directions and of unit thickness in the z direction. It is also assumed that the epicardium is represented by the plane at $z = 0$ which is also assumed insulated to facilitate a comparison with experimental data [13]. Further, the endocardium is represented by the plane at $z = 1$ which is in contact with a volume of blood extending to ∞ in the positive z direction.

To include the effect of both the intracellular and extracellular regions, the bidomain model [3], [14], [15] for cardiac tissue will be used. In order to solve the two bidomain equations, governing the intracellular potentials, ϕ_i and the extracellular potentials, ϕ_e, respectively, the transmembrane potential, $\phi_m = \phi_i - \phi_e$ is introduced. It can be shown that [14], [15] the governing equation for ϕ_e is

$$\nabla \cdot (\mathbf{M}_i + \mathbf{M}_e)\nabla\phi_e = -\nabla \cdot \mathbf{M}_i \nabla\phi_m \tag{1}$$

where $\mathbf{M}_e$ and $\mathbf{M}_i$ are conductivity tensors reflecting the anisotropy of the cardiac tissue. Hence, ϕ_e, can be determined from a knowledge of the transmembrane potential distribution, a quantity which is known from individual cell action potentials. Here, (1) will be solved to obtain the epicardial potential distribution, i.e., the value of ϕ_e at $z = 0$.

Finally, in the blood, being a source free region, the electric potential, ϕ_b, is governed by Laplace's equation

$$\nabla^2 \phi_b = 0. \tag{2}$$

B. Conductivity Tensor

Cardiac tissue is an electrically anisotropic structure, consisting of sheets of parallel strands of cells. It is well known that it is much easier for electric current to flow along the fibers than across them, both in the intracellular and extracellular domains. Hence, four values for conductivity are required: σ_l^i, σ_t^i, σ_l^e, σ_t^e where the superscripts i and e refer to the intracellular and extracellular domains, respectively, and the subscripts l and t refer to the longitudinal and transverse directions, respectively. Here, longitudinal means along the direction of the fibers and transverse means across the fibers, perpendicular to the longitudinal direction within a sheet. It is further assumed that the conductivity in the z direction, i.e., perpendicular to the sheets, is the same as in the transverse direction. Thus, this formulation ignores the secondary effects of sheet structure.

Other investigators have observed that the main fiber axis rotates in a counterclockwise direction as one moves from the epicardium to the endocardium. Reported rotations in the left ventricle are in the range of $103 \pm 21°$ [16] to a mean of 120° with extremes of 180°[17]. It is further assumed that the rotation varies linearly with depth [18]. Hence, if it is assumed that the fibers on the epicardium are aligned along the positive x axis, then the longitudinal direction at any depth z, with respect to the positive x axis can be given by

$$g(z) = \frac{2\pi}{3} z. \tag{3}$$

Given the above discussion, it follows that conductivities in the governing bidomain (1) must be represented as 3×3 matrices of the following form:

$$\mathbf{M}_n(x,y,z) = \begin{pmatrix} (\sigma_l^n - \sigma_t^n)\, c^2 + \sigma_t^n & (\sigma_l^n - \sigma_t^n)\, cs & 0 \\ (\sigma_l^n - \sigma_t^n)\, cs & (\sigma_l^n - \sigma_t^n)\, s^2 + \sigma_t^n & 0 \\ 0 & 0 & \sigma_t^n \end{pmatrix} \tag{4}$$

where $n = i$ or e (for intracellular and extracellular), $c = \cos g(z)$ and $s = \sin g(z)$.

The imburcation angle (the angle of inclination of the fibers relative to the epicardial surface) is assumed to be zero in this model, which is a reasonably common assumption [19]. Generally, this angle is less than 5° in the bulk of the myocardium [20] except in the regions of the apex and the base. Since the geometry of the model considered here better approximates the ventricular wall, the above assumption is not unreasonable.

C. Region of Subendocardial Ischaemia

It will be assumed that the ischaemic tissue occupies a finite region in the x and y directions, centered on the z axis. In the z direction, the region is bounded by the endocardium but does not extend to the epicardium (as this would then be full-thickness ischaemia). Hence, the ischaemic region can be described as

$$\mathcal{I} = \{(x,y,z) | -a_x \le x \le a_x, -a_y \le y \le a_y, a_z \le z \le 1\}. \tag{5}$$

However, as will be discussed later, the region does not necessarily have a sharp boundary, as indicated by the set $\mathcal{I}$. If the presence of a so-called ischaemic boundary is assumed, then there is a smooth transition between ischaemic and normal tissue. In this case, the quantities a_x, a_y and a_z (all measured in cm) represent centers of the ischaemic boundary.

To specify an analytic representation for the ischaemic region, the product representation for the transmembrane potential distribution

$$\phi_m(x,y,z) = \Delta\phi_p \Psi(x)\Psi(y)\Psi(1-z) \tag{6}$$

suggested by Tung [14] is employed. Here, $\Delta\phi_p$ is the difference in plateau potentials between normal and ischaemic tissue.

In any particular direction, t, the shape function, $\Psi(t)$, is defined by

$$\Psi(t) = \begin{cases} \frac{1-e^{-a_t/\lambda_t}\cosh\frac{t}{\lambda_t}}{1-e^{-a_t/\lambda_t}} & |t| \le a_t \\ \frac{e^{-|t|/\lambda_t}\sinh\frac{a_t}{\lambda_t}}{1-e^{-a_t/\lambda_t}} & |t| > a_t \end{cases} \quad (7)$$

where t is x , y or z. The parameters λ_t, $(t = x, y, z)$ govern the width of the ischaemic boundary and will be discussed below in Section II-G. Note that in (7), the argument of the shape function in the z direction is $1 - z$, to achieve the ischaemic region near the endocardium ($z = 1$).

D. Boundary Conditions

Solving differential equations (1) and (2) requires a set of boundary conditions. Since it is assumed that the cardiac tissue and the region of blood in contact with it are infinite in both the x and y directions, the potentials at large distances from the origin are set to zero, that is, as $x \to \pm\infty$ and $y \to \pm\infty$, $\phi_e = \phi_b = 0$. The assumption that the epicardium is in contact with an insulating medium means that

$$\text{at } z = 0; \frac{\partial \phi_e}{\partial z} = 0. \quad (8)$$

Further, at the interface between the tissue and the blood, there is continuity of potential and current, i.e.,

$$\text{at } z = 1; \phi_e = \phi_b \text{ and } \sigma_b \frac{\partial \phi_b}{\partial z} = \sigma_t^e \frac{\partial \phi_e}{\partial z} \quad (9)$$

where σ_b is the conductivity of blood. Finally, since the blood mass is assumed infinite in the positive z direction, $\phi_b = 0$ as $z \to \infty$.

E. Solution Method

The model proposed is three-dimensional (3-D) in a rectangular coordinate system and the governing (1) can be expanded to give

$$\begin{aligned} &\left(M_i^{11} + M_e^{11}\right)\frac{\partial^2 \phi_e}{\partial x^2} + 2\left(M_i^{12} + M_e^{12}\right)\frac{\partial^2 \phi_e}{\partial x \partial y} \\ &\quad + \left(M_i^{22} + M_e^{22}\right)\frac{\partial^2 \phi_e}{\partial y^2} + \left(M_i^{33} + M_e^{33}\right)\frac{\partial^2 \phi_e}{\partial z^2} \\ &\quad = -M_i^{11}\frac{\partial^2 \phi_m}{\partial x^2} - 2M_i^{12}\frac{\partial^2 \phi_m}{\partial x \partial y} - M_i^{22}\frac{\partial^2 \phi_m}{\partial y^2} \\ &\quad - M_i^{33}\frac{\partial^2 \phi_m}{\partial z^2} \end{aligned} \quad (10)$$

where M_n^{mj} represent the elements of the conductivity tensor matrices $\mathbf{M}_n$ $(n = i, e)$. It should be remembered that M_n^{11}, M_n^{12} and M_n^{22} $(n = i, e)$ are functions of z, through the fiber rotation, yet M_n^{33} $(n = i, e)$ are constant.

To solve (10) the ideas suggested by Tung [14] are extended by introducing the two-dimensional (2-D) Fourier transforms

$$\Phi_e(k, l, z) = \int_{-\infty}^{\infty}\int_{-\infty}^{\infty} \phi_e(x, y, z) e^{-2\pi i k x} e^{-2\pi i l y} dx dy \quad (11)$$

and

$$\Phi_m(k, l, z) = \int_{-\infty}^{\infty}\int_{-\infty}^{\infty} \phi_m(x, y, z) e^{-2\pi i k x} e^{-2\pi i l y} dx dy. \quad (12)$$

Applying these transformations to (10) gives the following ordinary differential equation in z:

$$\left(M_i^{33} + M_e^{33}\right)\frac{d^2\Phi_e}{dz^2} - h(z)\Phi_e = p(z)\Phi_m - M_i^{33}\frac{d^2\Phi_m}{dz^2} \quad (13)$$

where

$$\begin{aligned} h(z) = {} & 4\pi^2 k^2\left(M_i^{11} + M_e^{11}\right) + 8\pi^2 kl\left(M_i^{12} + M_e^{12}\right) \\ & + 4\pi^2 l^2\left(M_i^{22} + M_e^{22}\right) \end{aligned} \quad (14)$$

and

$$p(z) = 4\pi^2 k^2 M_i^{11} + 8\pi^2 klM_i^{12} + 4\pi^2 l^2 M_i^{22}. \quad (15)$$

By similarly defining $\Phi_b(k, l, z)$, application of the Fourier transformation to (2) yields

$$\frac{d^2\Phi_b}{dz^2} - 4\pi^2(k^2 + l^2)\Phi_b = 0. \quad (16)$$

This equation can be solved to give

$$\Phi_b = \beta e^{-2\pi\sqrt{k^2+l^2}z} \quad (17)$$

where the fact that $\Phi_b \to 0$ as $z \to \infty$ has been used and β is a constant to be determined.

Equation (13) can now be solved, for all pairs (k, l), using a simple finite difference approach over the interval $[0, 1]$ on the z axis. To achieve the solution it is necessary to utilize the conditions that

$$\text{at } z = 0; \frac{d\Phi_e}{dz} = 0 \quad (18)$$

and

$$\text{at } z = 1; \Phi_e = \Phi_b \text{ and } \sigma_b \frac{d\Phi_b}{dz} = \sigma_t^e \frac{d\Phi_e}{dz}. \quad (19)$$

The interval from $z = 0$ to $z = 1$ is discretised into a nonuniform grid of 100 points, clustered in the vicinity of the ischaemic border. This results in a tridiagonal system of algebraic equations which are solved using the routine "tridag" from Numerical Recipes [21].

Since only the epicardial potentials are of interest in this study, (13) is only solved for the value of Φ_e at $z = 0$. These values are collected into a 2-D array for various values of k and l which is inverted using a fast Fourier transform (FFT) routine [21] to recover the epicardial potential distribution. The fact that an inverse FFT has been used slightly changes the physics of the problem under consideration. Instead of dealing with a domain which is infinite in the x and y directions, the domain is now of finite extent and the boundary conditions are of an insulating type. In order to minimize the difference between these two situations, the computational domain must be large enough to allow the boundary potentials to approach zero. The assumption of a finite block of tissue would be required if any other numerical method (for example, 3-D finite difference or finite-element methods) were used.

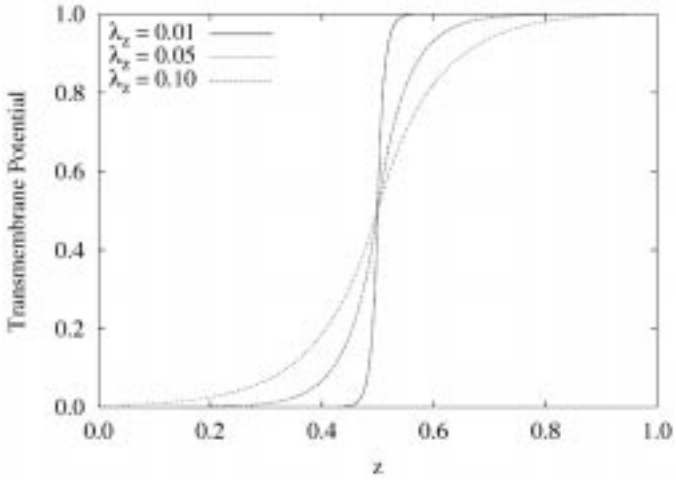

Fig. 1. Transmembrane potential distribution in the z direction for various thicknesses of the ischaemic boundary. A sharper transition occurs at smaller values of λ_z.

There are two quantities that require further comment in (13). First, Φ_m can be calculated readily as a product of one-dimensional Fourier transforms, for example

$$\int_{-\infty}^{\infty} \Psi(x) e^{-2\pi i k x} dx = \frac{\sin 2\pi k a}{1 - e^{-a/\lambda_x}} \frac{1}{\pi k \left(1 + 4\pi^2 k^2 \lambda_x^2\right)}. \tag{20}$$

Second, the derivative term $d^2\Phi_m/dz^2$ can be calculated analytically by differentiating the shape function $\Psi(1-z)$ twice with respect to z and multiplying by the Fourier transforms of $\Psi(x)$ and $\Psi(y)$.

F. Modeling Parameters

The conductivity values chosen for this paper are based on those presented by Clerc [22] and taken from Trayanova *et al.* [10]: $\sigma_l^i = 0.00174$ S/cm, $\sigma_l^e = 0.00625$ S/cm, $\sigma_t^i = 0.000193$ S/cm and $\sigma_t^e = 0.00236$ S/cm. The conductivity of blood, σ_b, is taken as 0.0067 S/cm. The block of tissue modeled was 1 cm thick and 16 cm in each of the x and y directions. Finally, the difference between plateau potentials in normal and ischaemic tissue, $\Delta\phi_p$, was set at -30 mV.

G. Boundary of the Ischaemic Region

The boundary of the ischaemic region represents the transition region between normal and ischaemic tissue. On a cellular level it would be expected that a normal cell could be juxtaposed with an ischaemic cell, but there is nothing to suggest that this is true on a macro scale. Therefore, in order to account for what could be considered a ragged border on a cellular level, the ischaemic boundary concept is included. The width of the ischaemic boundary is governed by the parameters λ_t, $(t = x, y, z)$ in (7). In the limiting case of any of these parameters going to zero, the result is a sharp ischaemic boundary in that particular direction.

As an example, the normalized transmembrane potential in the z direction, $\Psi(1-z)$, is shown in Fig. 1 for three values of λ_z equal to 0.01, 0.05, and 0.1 and $\Delta\phi_p = 1$. In all cases, the center of the ischaemic boundary is at $z = 0.5$. For $\lambda_z = 0.01$, there is a sharp change between normal tissue (left-hand side of the figure) and ischaemic tissue (right-hand side). The actual border extends over the region $0.45 \leq z \leq 0.55$. When the value of λ_z is increased to 0.05, the boundary is now the region $0.2 \leq z \leq 0.8$ and for $\lambda_z = 0.1$, the border extends across the entire thickness of the muscle.

If the degree of subendocardial ischaemia was increased to 75% (i.e., the center of the ischaemic boundary in the z direction was moved to $z = 0.25$), then for λ_z equal to 0.05 and 0.1, there would be a nonuniform transmembrane potential distribution set up on the epicardium which, as will be seen in Section III, affects the epicardial potential distribution.

Changing the value of λ_x and λ_y independently will not result in significant changes in the epicardial distribution. In Section III, the three values λ_x, λ_y, and λ_z, will always satisfy $\lambda_x = \lambda_y = \lambda_z = \lambda$. Also, the three values of λ_z indicated above will be used to study the differences between narrow, wide and intermediate ischaemic boundaries.

III. Results

A. Simplifications

It is possible to introduce several simplifications in the model in order to achieve analytic solutions to (13). These simplifications include ignoring the fiber rotation and assuming equal anisotropy ratios (where the ratio of the conductivities parallel and perpendicular to the fibers are the same in the intracellular and extracellular spaces).

First, assume that fiber rotation can be ignored. It then follows that the conductivity tensors can be expressed as diagonal matrices containing constant elements. Therefore, the mixed derivative terms in (10) disappear and all other coefficients in the differential equation are constant. In turn, the coefficients appearing in the ordinary differential equation for Φ_e (13) are again constant. In this case, (13) can be solved via the method of variation of parameters and hence an analytic solution can be obtained for Φ_e, assuming the integrals required in the variation of parameters can be evaluated.

On the other hand, if it is assumed that the anisotropy ratios are equal, it can be shown that (13) reduces to a homogeneous differential equation with nonconstant coefficients, which is most readily solved via a numerical technique given the functional form of the coefficient function $p(z)$.

However, if both of the above assumptions are used, then an over-simplification results. It can be shown that (13) reduces to a homogeneous differential equation with constant coefficients which is readily solved analytically. The over-simplification arises because the resulting epicardial potential distribution depends only on the epicardial transmembrane potential distribution and its normal derivative. Interpreting this result physically means that, for a uniform transmembrane potential distribution on the epicardium, the position of the ischaemic boundary within the myocardium will not affect the epicardial potential distribution. That is to say, the degree of subendocardial ischaemia will not become apparent until the ischaemia is nearly full thickness which is demonstrated in Fig. 2. In this figure, the epicardial potential distributions are identical

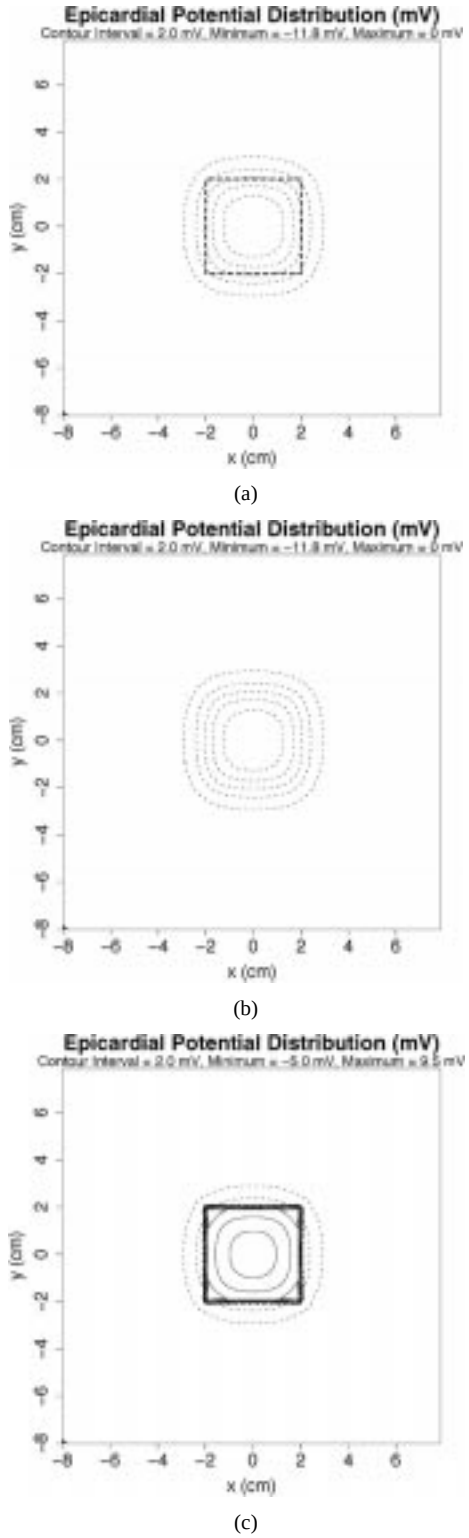

Fig. 2. Epicardial potential distributions for varying degrees of subendocardial ischaemia with isotropic cardiac tissue and an ischaemic region of 16 cm^2. Dotted lines indicate negative potentials, with positive potentials indicated by thin solid lines. The thick solid line indicates the zero potential. The thick dashed line in (a) represents the projection of the ischaemic region onto the epicardium (this regions is common to all subsequent contour plots). The contour interval in each plot is 2.0 mV. (a) 10%, (b) 90%, and (c) 100% ischaemia.

for subendocardial ischaemia up to 90% of the thickness of the myocardium. Experimental evidence has shown that this is not the case [13].

B. Conduction Anisotropy Without Fiber Rotation

Fig. 3 shows the contour plots of the epicardial ($z = 0$) potential distribution as the degree of subendocardial ischaemia increases from 10% to full thickness. The ischaemic region is centered on the z axis with an area of 16 cm^2 and the fibers are directed parallel to the x axis. Finally, the parameter describing the ischaemic border is $\lambda = 0.01$.

As perhaps would be expected, the potential distribution for small degrees of ischaemia shows a set of elliptical level curves in a valley (ST depression) oriented along the direction of the fibers. This underlying pattern does not change as the degree of ischaemia increases. However, as the degree of ischaemia does increase, two, and eventually three, distinct valleys appear, all in a line oriented along the fiber direction. The two outer valleys intensify further as the degree of ischaemia increases, with the central valley eventually becoming a peak (ST elevation) at approximately 80% ischaemia. Also, at higher degrees of ischaemia there are large potential gradients above the two ischaemic borders perpendicular to the direction of the fibers.

C. Conduction Anisotropy With Fiber Rotation

Now consider the block of tissue to have conduction anisotropy combined with a fiber rotation of 120° from the epicardium to the endocardium. As above, the fibers on the epicardium are directed parallel to the x axis. Fig. 4 shows a contour plot of the epicardial ($z = 0$) potential distribution as the degree of subendocardial ischaemia increases from 10% to full thickness. Again the ischaemic region is centered on the z axis with an area of 16 cm^2. The parameter describing the ischaemic border is again $\lambda = 0.01$.

With 10% subendocardial ischaemia a single elliptical valley exists in the epicardial potential distribution with the long axis of the valley aligned approximately along the x axis. This would suggest ST depression on the epicardium above the ischaemic region. At 20% subendocardial ischaemia (not shown), the depth of the valley has reduced and it is now directed with a long axis rotated counterclockwise through about 90°, which is due to the fiber rotation. At 30% ischaemia two distinct valleys (again shallower) are apparent in the epicardial potential distribution and at 40% ischaemia (not shown) they are deeper again with a considerable ridge between them. Here, there are significant potential gradients above what would be the borders of the ischaemic region in the longitudinal direction of the fibers on the endocardium. Between 40% and 50% ischaemia the ridge between the two valleys (which are again deeper) becomes positive and there would be ST elevation occurring between the two valleys of ST depression. As the degree of subendocardial increases further to 70% and 90%, this pattern is maintained with the valleys becoming deeper and the ridge between higher. Finally, at full thickness, the ridge is a spike with ST depression occurring only near the boundary of the ischaemic region.

D. Effect of the Ischaemic Boundaries

Fig. 5 shows the effect of changing the width of the ischaemic boundary. The three values of λ_z shown in Fig. 1 coincide with the three values of λ used in these simulations. In each case,

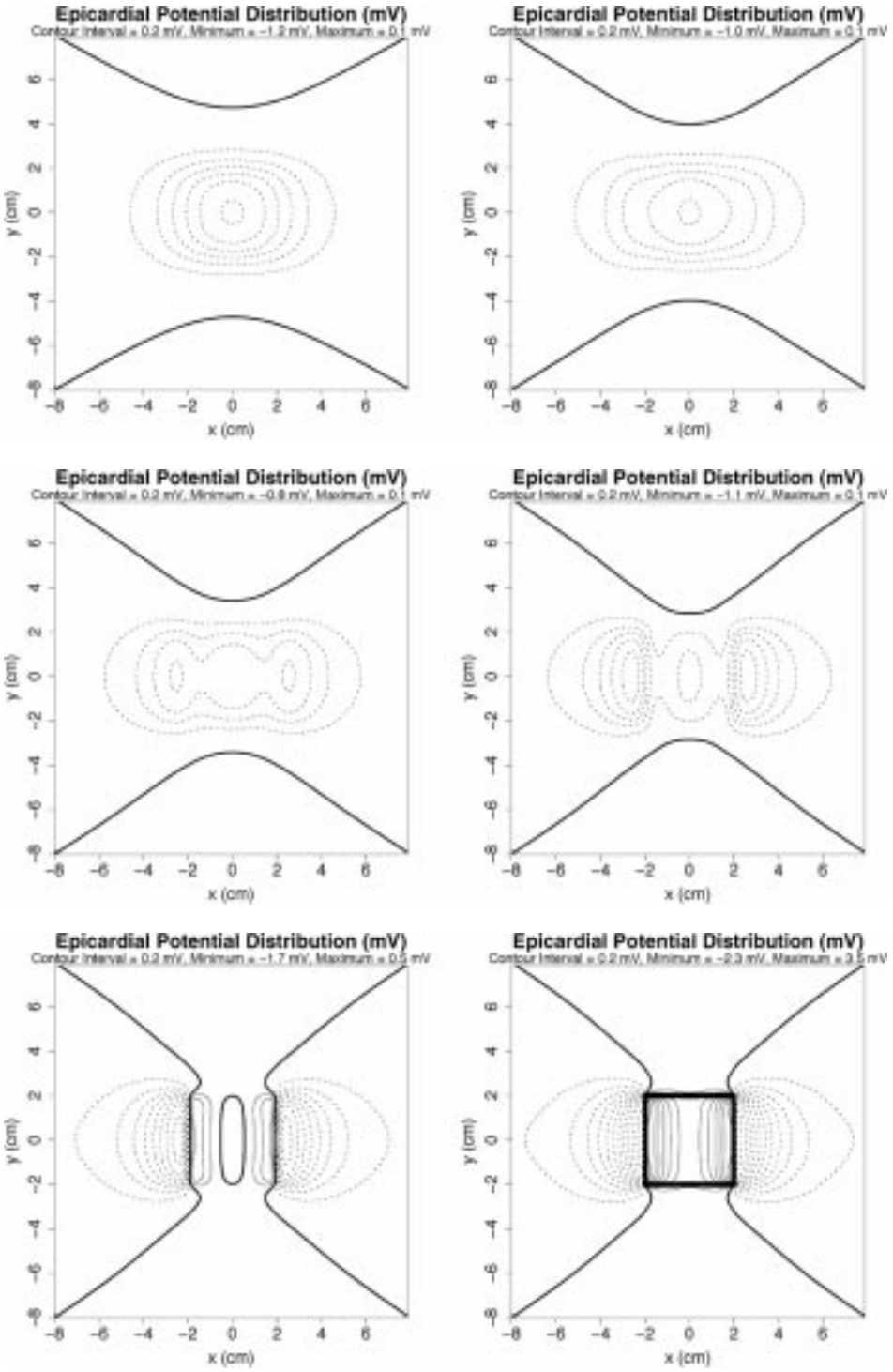

Fig. 3. Epicardial potential distributions for varying degrees of subendocardial ischaemia with anisotropic cardiac tissue without fiber rotation and an ischaemic region of 16 cm^2. The format for each figure is described in the caption for Fig. 2. The contour interval in each plot is 0.2 mV. (a) 10%, (b) 30%, (c) 50%, (d) 70%, (e) 90%, and (f) 100% ischaemia.

the area of the ischaemic region is 16 cm^2 and contour plots are shown for 50% and 75% subendocardial ischaemia. At 50% ischaemia (left-hand column), increasing the width of the ischaemic boundary does not have a great effect on the potential contours, except that the valleys become shallower. This is perhaps not surprising because, as can be seen from Fig. 1, the transmembrane potential on the epicardium is very close to zero in all cases.

However, at 75% subendocardial ischaemia, some differences do emerge (that is to say, in Fig. 1 the center of the ischaemic region (where the dimensionless transmembrane potential is 0.5) has been moved to $z = 0.25$). In this case, the transition region intersects the epicardium resulting in regions of nonzero transmembrane potential on the epicardial surface for $\lambda = 0.05$ and $\lambda = 0.1$. The result of this, as demonstrated in Fig. 5, is higher peaks and shallower valleys of the corresponding contour plots.

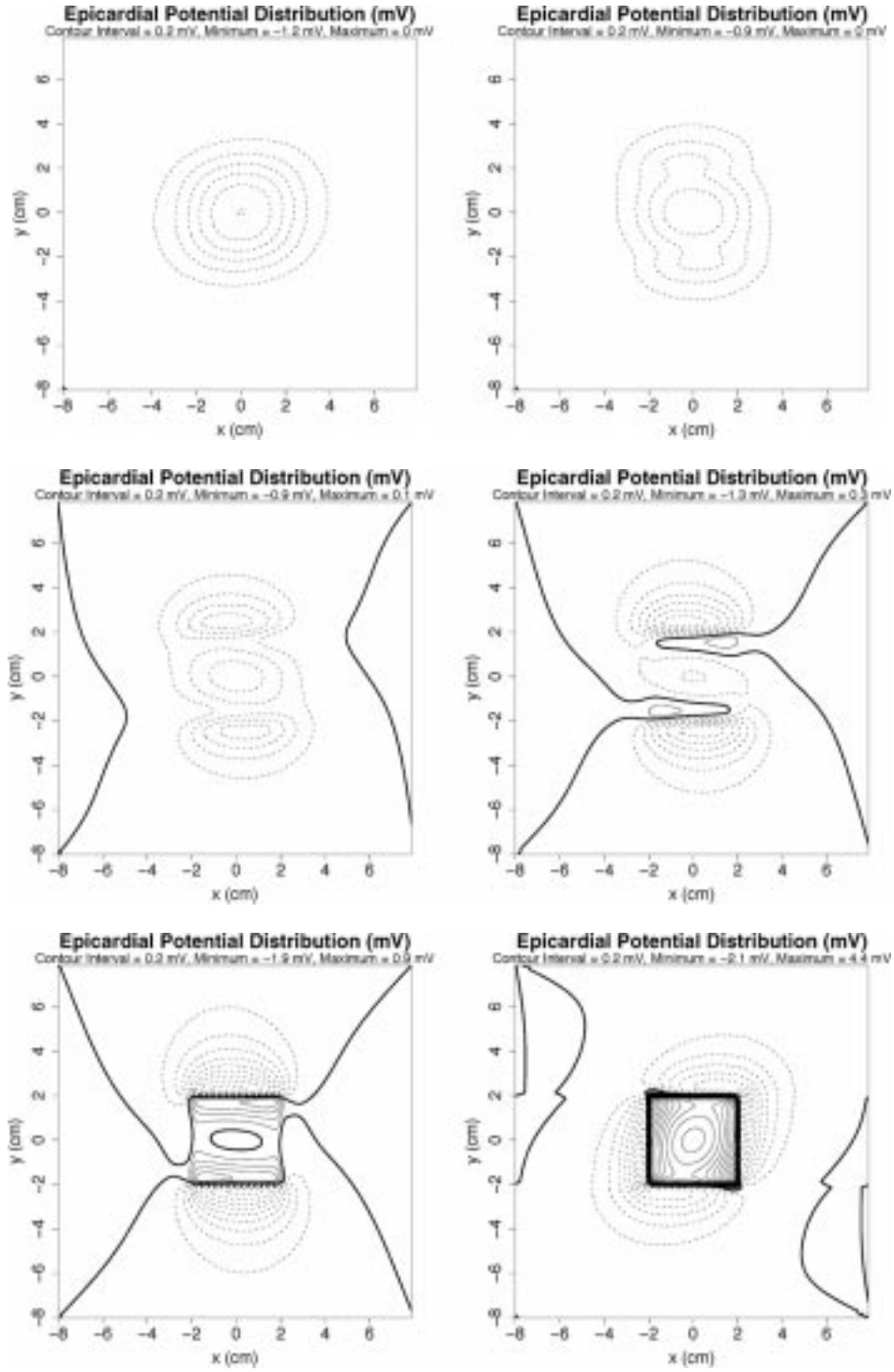

Fig. 4. Epicardial potential distributions for varying degrees of subendocardial ischaemia with anisotropic cardiac tissue with fiber rotation and an ischaemic region of 16 cm^2. The format for each figure is described in the caption for Fig. 2. The contour interval in each plot is 0.2 mV. (a) 10%, (b) 30%, (c) 50%, (d) 70%, (e) 90%, and (f) 100% ischaemia.

Hence, increasing the width of the ischaemic boundary tends to indicate that ST elevation would become apparent at lesser degrees of subendocardial ischaemia.

IV. Discussion

This paper has introduced a bidomain model to study the ST segment epicardial potential distributions induced by subendocardial ischaemia. Realistic conductivities have been used and the rotation of cardiac fibers from the endocardium to the epicardium has also been included.

Briefly, simulations have shown that in the transition from partial to full-thickness ischaemia there is initially ST depression over the ischaemic region with a region of ST elevation developing in the center as the degree of ischaemia increases. Finally, at full-thickness ischaemia there is ST elevation over

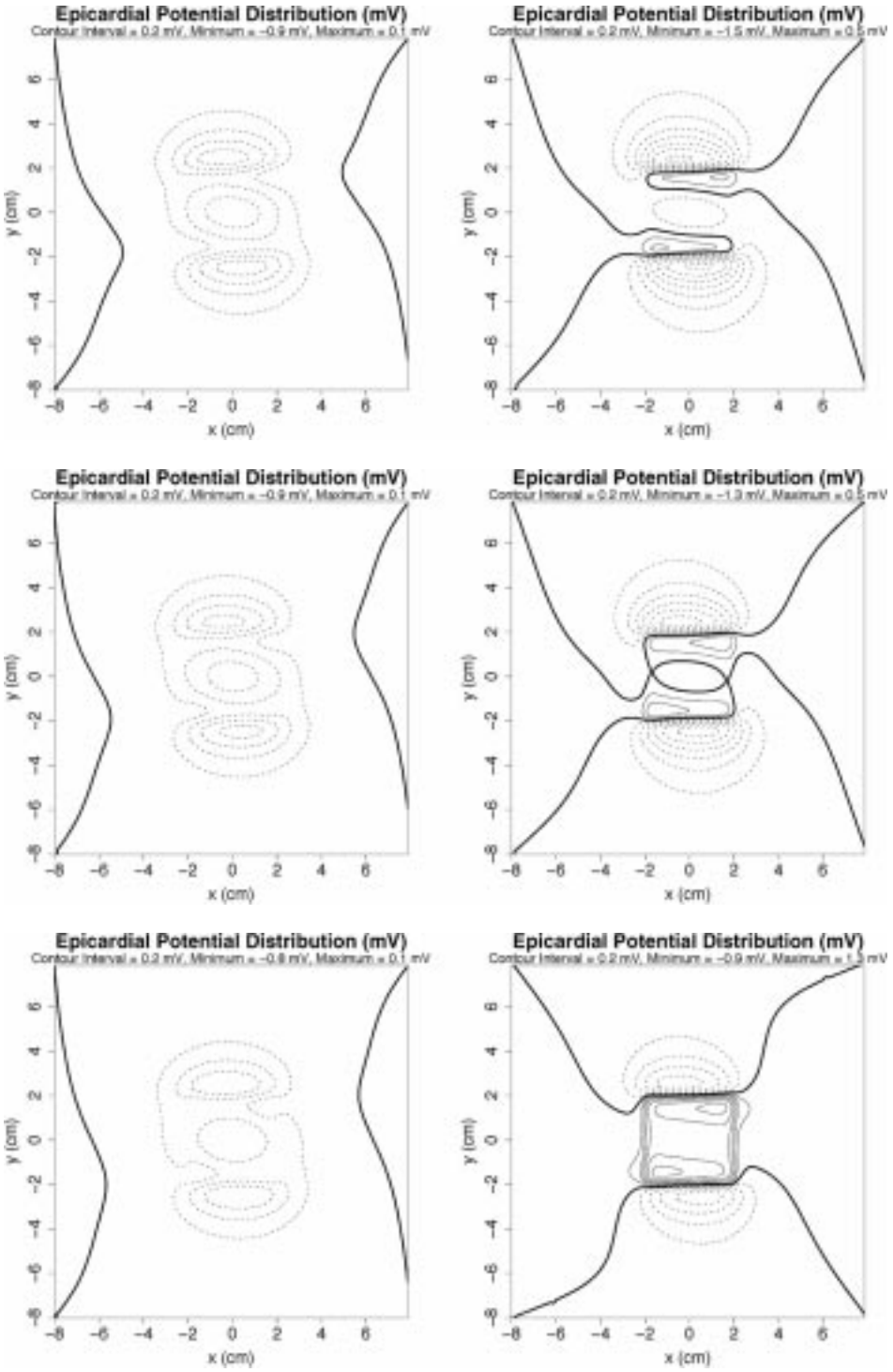

Fig. 5. Epicardial potential distribution at 50% and 75% subendocardial ischaemia at various thicknesses of the ischaemic boundary. The format for each figure is described in the caption for Fig. 2. The contour interval in each plot is 0.2 mV. (a) 50% subendocardial ischaemia, $\lambda = 0.01$; (b) 75% subendocardial ischaemia, $\lambda = 0.01$; (c) 50% subendocardial ischaemia, $\lambda = 0.05$; (d) 75% subendocardial ischaemia, $\lambda = 0.05$; (e) 50% subendocardial ischaemia, $\lambda = 0.1$; (f) 75% subendocardial ischaemia, $\lambda = 0.1$

the region of ischaemia (greater near the boundary) and ST depression just outside the boundary. The model also predicts large potential gradients above the boundary of the ischaemic region. As the width of the ischaemic boundary in the transmural direction increases, ST elevation appears at a lesser degree of subendocardial ischaemia.

Although this is a simple model, based on fairly restrictive assumptions (in order to accommodate the mathematics), it does reflect some of the experimental observations published previously, as well as some desirable features of other simpler models. On the other hand, there are several experimentally observed features that this model does not predict.

First, consider the limitations of the model. The main limitation is that the model does not support the experimental observations of Li *et al.* [13] that epicardial depression does not predict the position of the ischaemic region. Clearly, from Figs. 2–4, the ST depression observed at small degrees of subendocardial ischaemia is above the region of ischaemia. The experiments of Li *et al.* [13] were performed using the sheep model and subendocardial ischaemia was induced by partially occluding the left circumflex or left anterior descending coronary arteries. Such occlusion induces ischaemia over approximately half of the left ventricle in each case and there is little overlap between the two regions. The observation was that the epicardial potential distributions were very similar for occlusion of the respective arteries (correlation coefficient of 0.77 ± 0.14 using six animals). A possible explanation for the discrepancy between the experiment and model is that the model is an infinite slab of cardiac tissue attached to an infinite amount of blood, whereas, clearly, the experimental model dealt with finite quantities. Also, the experimental model induced ischaemia from the middle of the left-ventricular free wall to the septum behind which is another blood mass. Given this and the size of the ischaemic region, there is a clear difference in the geometries being considered, as well as the relative size of the ischaemic region (it is effectively assumed small in the mathematical model).

The simple model of ST depression presented here predicts many features observed in experimental studies of ST depression. First, consider full-thickness ischaemia results (bottom right-hand panels of Figs. 2–4). In each case, the highest amplitude of ST elevation was obtained at the boundary of the ischaemic region, as was observed by Li *et al.* [23] with ligation of the LAD and LCX arteries. However, this behavior was not observed with the occlusion of the obtuse marginal artery, nor was it observed in the experimental studies of Smith *et al.* [12] where a more convex distribution was observed. Interestingly, though, by changing the width of the ischaemic border in the x and y directions so that $\lambda_x = \lambda_y = 0.5$ (with $\lambda_z = 0.01$), epicardial potential distributions of the type observed by Smith *et al.* were obtained (see Fig. 6). That is, in this case, the maximum of the potential distribution was obtained more toward the center of the ischaemic region. The model also predicts ST depression just outside the ischaemic boundary and this depression increases in magnitude as the size of the ischaemic region increases. This fact was also observed by Li *et al.* [23]. Model predictions also fit with the simple model of Holland and Brooks [11].

As observed experimentally by Li *et al.* [13] in the sheep model, the ST depression increases before the occurrence of ST elevation and continues to increase as the ST elevation increases. The same observations have also been reported in a study by Guyton *et al.* [24] using the canine model. The main difference between the model and experimental observations is that the model predicts initial ST elevation near the ischaemic border and not the ischaemic center. There is also a discrepancy in the magnitudes of the ST depression between the model and the experimentally recorded data. A possible explanation for this is that the experiments are performed in a closed, finite structure which is ultimately insulated. On the other hand, the modeling was performed in a semi-infinite domain, where

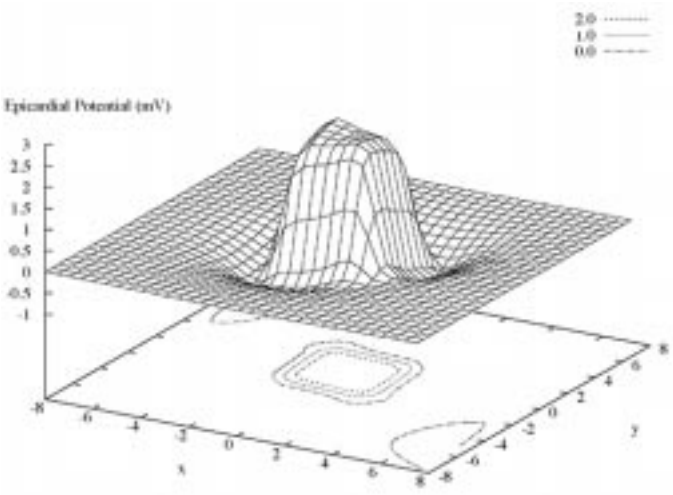

Fig. 6. Epicardial potential distribution for full-thickness ischaemia with an ischaemic boundary characterized by $\lambda_x = \lambda_y = 0.5$ and $\lambda_z = 0.01$. Contour values (in mV) are indicated on the figure.

the cardiac tissue was attached to a very large amount of blood, which provides an enormous potential sink. The effect of this sink would be to lower the observed potentials on the epicardial surface.

In a recent combined simulation/experimental study [13], a realistically shaped human heart provided the basis for the modeling studies. The governing bidomain equations were solved with the finite-element method, however, rotation of the cardiac fibers was ignored. Also, the current source due to the ischaemic boundary was treated as a volumetric source in one layer of cells on one side of the boundary and as a volumetric sink in one layer of cells on the other side of the boundary (to simulate a dipole layer). The fact that this model, with its lack of fiber rotation, more accurately predicts the experimentally observed epicardial potentials than the current model with fiber rotation, poses an interesting question. Clearly, the above arguments regarding differing geometry could provide part of the explanation. However, a combined analytical/numerical study of the problem in a simple geometry could also provide further insights into the differences.

Now consider the transition from subendocardial ischaemia to full-thickness ischaemia as shown in Figs. 2–4. A major difference between these simulations is the degree of subendocardial ischaemia at which ST elevation appears above the ischaemic region. In the isotropic case, it only appears when the ischaemia is nearly full thickness and for the anisotropic case without fiber rotation it occurs at about 80% ischaemia. Yet, when fiber rotation is included ST elevation appears at about 55%. Another difference between the models is in the magnitude of the observed epicardial potentials where, for the isotropic model the potentials are up to a factor of ten higher than for the other two models which are of similar magnitudes. In the two models with anisotropy included, from the different directions of the elliptical level curves, the model without fiber rotation has a longer major axis than the model with fiber rotation at all degrees of subendocardial ischaemia. A possible explanation for these two observations is that the fiber rotation (which introduces a nonuniform conductivity distribution

lacking uniform directional anisotropy) has the effect of pulling the elliptical potential distribution off its major axis on the epicardium and subsequently smoothing the observed potential distribution cardiac tissue.

The above observations are in contrast to the observations relating to the simplified isotropic case, where the epicardial potential distribution is the same for all degrees of subendocardial ischaemia until the edge of the ischaemic border hits the epicardial surface (see Fig. 2).

The study of the transition to full-thickness ischaemia when fiber rotation is included (Fig. 4) reveals a complex relationship between the fiber rotation and the degree of subendocardial ischaemia. This is especially evident when the subendocardial ischaemia is between 10% and 30% [Fig. 4(a) and (b)]. In this range, the major axis of the elliptical contours moves through an angle of about 90°. Such behavior must be due to the presence of the fiber rotation, because when fiber rotation is ignored, the major axis of the contours is in the same direction regardless of the degree of ischaemia (Fig. 3).

A more detailed examination of the transition (at increments of 1%) shows that the elliptical pattern with 10% ischaemia does not actually rotate through the 90° to obtain the elliptical pattern at 30% ischaemia, but becomes a circular pattern at about 17% before stretching out in the new direction as the degree of ischaemia increases. The pattern at 17% looks like that of an isotropic model. At this point, no explanation is offered for this behavior.

Changing the size of the ischaemic region has a number of effects on the epicardial potential distribution. Increasing the $x-y$ extent of the ischaemic region increases the magnitudes of the valleys and peaks; however, ST elevation is not observed until there is a greater degree of subendocardial ischaemia. For example, when the area of the ischaemic region is increased to 64 cm^2, ST elevation is not observed until the subendocardial ischaemia is nearly 70%. However, reducing the area of the ischaemic region to 4 cm^2 yields ST elevation before 50% subendocardial ischaemia. Otherwise, the epicardial potential distributions shown in Fig. 4 are fairly typical.

Finally, as observed in the studies of Smith *et al.* [12] and Li *et al.* [13], large potential gradients exist near the ischaemic border. This same feature is observed with the model. The magnitude of the gradients predicted by the model developed here lies between those predicted by the models of Holland and Brooks [11] (which are larger) and of Smith *et al.* [12] (which are smaller).

V. Conclusion

This paper has presented a simple bidomain model of cardiac tissue to study the behavior of ST depression and elevation in subendocardial and full-thickness ischaemia, as well as the transition between the two.

In this paper, both isotropic and anisotropic (with and without fiber rotation) models of cardiac tissue have been considered. The simplification of using isotropic cardiac tissue predicts identical epicardial potential distributions for all degrees of subendocardial ischaemia. This observation is in total contrast to experimental observations. Therefore, it must be concluded that the assumption of tissue isotropy is totally inadequate and greater realism must be included.

Using a model in which tissue anisotropy and fiber rotation are included predicts some of the features found in experimental studies of similar physical phenomena. Perhaps the most notable discrepancy between model and experiment is that the model does localize subendocardial ischaemia, in contrast to the observations of Li *et al.* [13]. However, geometrical considerations might provide a reason for this difference.

Although this model has been applied to a study of the epicardial potentials due to the presence of ischaemic tissue, the same techniques could be used to study depolarization wave fronts before epicardial breakthrough. Such a study could be effected by a change in the representation of the quantity $\nabla\phi_m$.

Acknowledgment

The authors would like to thank the three anonymous referees for their constructive suggestions and comments on this manuscript.

References

[1] C. C. Wolferth, S. Bettet, M. M. Livezey, and F. Murphy, "Negative displacement of the RS-T segment in the electrocardiogram and its relationships to positive displacement: An experimental study," *Amer. Heart J.*, vol. 29, pp. 220–244, 1945.

[2] H. Toyoshima, A. Ekmekci, E. Flamm, Y. Mizuno, T. Nagaya, R. Nakayama, K. Yamada, and M. Prinzmetal, "Angina pectoris VII. The nature of ST depression in acute myocardial ischaemia," *Amer. J. Cardiol.*, vol. 13, pp. 498–509, 1964.

[3] O. H. Schmitt, "Biological information processing using the concept of interpenetrating domains," in *Information Processing in the Nervous System*, K. N. Leibovic, Ed. New York: Springer-Verlag, 1969, ch. 18, pp. 325–331.

[4] N. A. Trayanova, C. S. Henriquez, and R. Plonsey, "Limitations of approximate solutions for computing the extracellular potential of single fibers and bundle equivalents," *IEEE Trans. Biomed. Eng.*, vol. 37, pp. 22–35, Jan. 1990.

[5] B. J. Roth, "Action potential propagation in a thick strand of cardiac muscle," *Circ. Res.*, vol. 68, no. 1, pp. 162–173, Jan. 1991.

[6] C. S. Henriquez and R. Plonsey, "Simulation of propagation along a cylindrical bundle of cardiac tissue—I: Mathematical formulation," *IEEE Trans. Biomed. Eng.*, vol. 37, pp. 850–860, Sept. 1990.

[7] ——, "Simulation of propagation along a cylindrical bundle of cardiac tissue—II: Results of simulation," *IEEE Trans. Biomed. Eng.*, vol. 37, pp. 861–875, Sept. 1990.

[8] D. B. Geselowitz, S. Smith, K. Mowrey, and E. J. Berbari, "Model studies of extracellular electrograms arising from an excitation wave propagating in a thin layer," *IEEE Trans. Biomed. Eng.*, vol. 38, pp. 526–531, June 1991.

[9] M. Lorange and R. M. Gulrajani, "A computer heart model incorporating anisotropic propagation: I. Model construction and simulation of normal activation," *J. Electrocardiol.*, vol. 26, no. 4, pp. 245–261, 1993.

[10] N. A. Trayanova, B. J. Roth, and L. J. Malden, "The response of a spherical heart to a uniform electric field: A bidomain analysis of cardiac stimulation," *IEEE Trans. Biomed. Eng.*, vol. 40, pp. 899–908, Sept. 1993.

[11] R. P. Holland and H. Brooks, "TQ-ST segment mapping: Critical review and analysis of current concepts," *Amer. J. Cardiol.*, vol. 40, pp. 110–129, 1977.

[12] G. T. Smith, G. G. Geary, W. Blanchard, T. H. Roelofs, W. Ruf, and J. J. McNamara, "An electrocardiographic model of myocardial ischaemic injury," *J. Electrocardiol.*, vol. 16, no. 3, pp. 223–234, 1983.

[13] D. Li, C. Y. Li, A. C. Yong, and D. Kilpatrick, "Source of electrocardiographic ST changes in subendocardial ischemia," *Circ. Res.*, vol. 82, pp. 957–970, 1998.

[14] L. Tung, "A Bi-Domain Model for Describing Ischaemic Myocardial D-C Potentials," Ph. D. dissertation, Massachusetts Inst. Technol., Cambridge, June 1978.

[15] W. T. Miller and D. B. Geselowitz, "Simulation studies of the electrocardiogram: I the normal heart," *Circ. Res.*, vol. 43, pp. 301–315, 1978.
[16] B. Taccardi, E. Macchi, R. L. Lux, P. R. Ershler, S. Spaggiari, S. Baruffi, and Y. Vyhmeister, "Effect of myocardial fiber direction on epicardial potentials," *Circulation*, vol. 90, pp. 3076–3090, 1994.
[17] D. D. Streeter, "Gross morrphology and fiber geometry of the heart ," in *Handbook of Physiology*, R. M. Berne, Ed. Baltimore, MD: Williams & Williams, 1979, vol. 1, The Cardiovascular System, ch. 2, pp. 61–112.
[18] P. C. Franzone, L. Guerri, and B. Taccardi, "Spread of excitation in a myocardial volume: Simulation studies in a model of anisotropic ventricular muscle activated by point stimulation," *J. Cardiovasc. Electrophysiol.*, vol. 4, no. 2, pp. 144–160, Apr. 1993.
[19] P. Colli-Franzone and L. Guerri, "Spreading of excitation in 3-D models of the anisotropic cardiac tissue I: Validation of the eikonal model," *Math. Biosci.*, vol. 113, pp. 145–209, 1993.
[20] I. J. Legrice, P. J. Hunter, and B. H. Smail, "Laminar structure of the heart: A mathematical model," *Amer. J. Physiol.*, vol. 272, pp. H2466–H2476, 1997.
[21] W. H. Press, B. P. Flannery, S. A. Teukolsky, and W. T. Vetterling, *Numerical Recipes, The Art of Scientific Computing*, 1st ed. Cambridge, U.K.: Cambridge Univ. Press, 1989.
[22] L. Clerc, "Directional differences of impulse spread in trabecular muscle from mammalian heart," *J. Physiol.*, vol. 255, pp. 335–346, 1976.
[23] D. Li, C. Y. Li, A. C. Yong, P. R. Johnston, and D. Kilpatrick, "Epicardial ST depression in acute myocardial infarction," *Circ. Res.*, vol. 85, pp. 959–964, 1999.
[24] R. A. Guyton, J. H. McClethan, G. E. Newman, and L. L. Michaelis, "Significance of subendocardial S-T segment elevation caused by coronary stenosis in the dog," *Amer. J. Cardiol.*, vol. 40, pp. 373–380, 1977.

Peter R. Johnston was born in Hobart, Tasmania, Australia, in 1960. He received the honors degree in mathematics from the University of Tasmania, Tasmania, Australia, in 1983, and the Ph.D. degree in the School of Chemical Engineering from the University of Queensland, Queensland, Australia, in 1987.

Thereafter, he worked in industry for three years before being employed as Senior Lecturer at the University of Tasmania, conjointly in the Departments of Medicine and Mathematics. He is now a Senior Lecturer in Mathematics at Griffith University, Brisbane, Queensland. His current areas of interest include the forward and inverse problems in electrocardiology, solution techniques for differential equations, and modeling blood flow using computational fluid dynamics.

David Kilpatrick received the B.Sc. (physics, mathematics), MBChB, and MD degrees from the University of Otago, Dunedin, Australia, in 1967, 1972, and 1981, respectively. He also received the MRCP (UK) and FRACP degrees in 1979 and 1983, respectively.

He is an unemployed physicist currently working as a Professor of Medicine in the University of Tasmania, Tasmania, Australia. He was a commonwealth scholar at the Royal Postgraduate Medical School, Hammersmith Hospital, London 1974–79 and received further clinical training at Dalhousie Nova Scotia, and the University of California San Francisco, before moving to Australia. His current interests include the origin of the electrocardiogram, coronary blood flow, and fiber-optic laser Doppler anemometry. Most of the time he works as a cardiologist.

Chuan Yong Li was born in Shanxi, China, in 1964. She received the B.S. and M.S. degrees, both in physics, from Nankai University, Tianjin, China, in 1984 and 1987, respectively. She received the Ph.D. degree in medical science from the University of Tasmania, Australia, in 1997.

From 1987–1992, she was working as a lecturer in Department of Biomedical Engineering, Tianjin Medical University, Tianjin, China. She is currently working as an Associate Professor in Department of Biophysics, School of Physics, Nankai University. Her research interests include biomedical signal processing and computer simulation in biomedical applications.